# The driver design for $N_2O$ gas detection system based on tunable interband cascade laser

*Lihuan* Liao[1,2], *Jingjing* Zhang[1], and *Daming* Dong[2,*]

[1]Anhui University, Hefei 230039, China
[2]Beijing Research Center for Intelligent Equipment for Agriculture, Beijing Academy of Agriculture and Forestry Sciences, Beijing 100097, China

**Abstract.** In this paper, the driver circuit for $N_2O$ gas detection system based on tunable interband cascade laser (ICL) is developed. Considering the influence of power supply stability on the digital-analog hybrid drive circuit of tunable diode laser absorption spectroscopy (TDALS), the high-efficiency TPS5430 is used to design the positive and negative power supply circuit. The large electrolytic capacitor + post-stage LC filter combination filter is used to effectively filter out high and low frequency ripple and switching noise. The use of thick high current trace + via + multilayer printed circuit board (PCB) design makes the line temperature rise smaller, more stable and durable, and uses high frequency shielding inductance to effectively reduce radiation interference to ensure the stability of the drive. The STM32F407, a high-performance microcontroller based on the ARM Cortex-M4 core, is used as the master control chip and generates a sawtooth scanning signal. The direct digital synthesizer (DDS) chip ICL8038 is used to generate a sinusoidal modulated signal of a specific frequency. The two signals are superimposed by a reverse addition circuit, and the laser drive signal is generated by a developed positive feedback balanced voltage-current conversion circuit. Experimental results show that the driver circuit can well meet the drive development requirements of $N_2O$ gas detection systems based on tunable interband cascade laser.

## 1 Introduction

Nitrous oxide ($N_2O$) is an important greenhouse gas with a single molecule warming potential of about 298 times that of carbon dioxide (IPCC, 2007), and it can remain in the atmosphere for a long time. It destroys the ozone layer, leading to the enhancement of solar ultraviolet radiation, directly causing harm to the human body[1-2]. As one of the natural components of the atmosphere, $N_2O$ is mainly derived from the process of soil microbial denitrification. Limited by soil nitrogen, the $N_2O$ released by denitrification under natural conditions is limited. However, human activities are increasing soil denitrification, leading to an increase in $N_2O$ emissions. Farmland soil has become the largest anthropogenic release source of atmospheric nitrous oxide[3-4]. Therefore, it is of great significance to achieve accurate measurement of nitrous oxide gas.

The interband cascade laser is a tunable semiconductor laser with advantages of high radiation efficiency, low power consumption, low threshold current, and long life[5-7]. The tunable diode laser absorption spectroscopy technique can be used to control the output wavelength of the semiconductor laser by controlling the current injected into the semiconductor laser or the temperature of the semiconductor laser, and the output wavelength is scanned through the gas to be measured to obtain the absorption spectrum of the gas to be tested, can realize high reliability and high precision of trace gases of non-contact detection[8-10].

In this paper, for the driving needs of $N_2O$ gas detection system of tunable interband cascade laser, STM32F407 is used as the master control chip, and its built-in DAC is used to generate the sawtooth scanning signal and the sinusoidal modulation signal generated by ICL8038. The superimposed signal is driven by the designed signal superposition and positive feedback balanced voltage-current conversion circuit to drive the laser.

## 2 Overall system design

The overall design block diagram of the ICL drive system is shown in Figure 1. The system mainly includes five parts: power supply circuit, signal generation circuit, signal superposition circuit and positive feedback balanced voltage-current conversion circuit and peripheral control and communication circuit. The power supply is a low ripple stable voltage source consisting of the TPS5430 and AMS1117. In the signal generation part, the internal 12-bit DAC is controlled by the microcontroller STM32F407 to output a 10Hz sawtooth wave signal, and the DDS chip ICL8038 generates a 10KHz sine wave signal. Signal superimposition and positive feedback balanced voltage-current conversion circuit, this part generates the current drive signal

* Daming Dong: damingdong@hotmail.com

required by ICL. The peripheral control and communication part completes the program download, output signal control and serial communication of STM32F407.

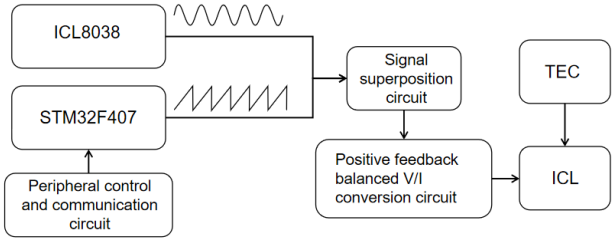


**Fig. 1.** The overall design block diagram of the ICL drive system.

## 3 Drive circuit design

### 3.1 Power circuit design

Semiconductor laser have poor current impact resistance, and small changes in current cause large changes in the output laser. Therefore, practical applications have high requirements on the stability and performance of the driving power supply. In order to ensure reliable and stable operation of the laser, a good power supply circuit is especially important.

The power circuit design part uses the high-performance DC/DC switching power conversion chip TPS5430 from Texas Instruments[11]. The TPS5430 has a wide input voltage range of 5.5V to 36V, up to 95% conversion efficiency, adjustable output voltage, and can be adjusted to a minimum of 1.22V. In addition, the TPS5430 features overcurrent protection, overvoltage protection, and thermal shutdown, and internal compensation minimizes the number of peripheral components, thus greatly simplifying the development of high-performance power supply circuits[12-13].

ICL drive system power supply design circuit shown in Figure 2. The AMS1117 part supplies power to the digital circuit part of the drive system, and the TPS5430 supplies power to the analog circuit part. U1 and U2 are TPS5430, U2 and U3 are AMS1117, and L1~L4 are integrated high-frequency shielding inductors, which can effectively reduce radiation interference. RP1 and RP2 are sliding rheostats. Adjusting RP1 and RP2 can provide a variety of positive and negative voltages. The power circuit adopts a thick high current trace + via + 4 layers PCB design, which makes the line temperature rise smaller, more stable and lasting. It uses large electrolytic capacitor + post-stage LC filter combination to filter, effectively filtering high and low frequency ripple and switching noise.

### 3.2 Signal generation circuit

The signal generating circuit is composed of a sawtooth signal generating portion and a sinusoidal signal generating portion. Among them, the sawtooth signal is generated by the built-in DAC of STM32F407[14-15]. The STM32F4XX series DAC module is a 12-bit voltage output digital-to-analog converter with two output channels, each of which can be converted individually or simultaneously. The DAC can be configured in either 12-bit or 8-bit mode and can be used with a DMA controller. In this design, the DAC is configured in 12-bit mode, the data is right-justified, and DAC channel 1 is used, sharing an input reference voltage pin $V_{REF+}$ with the ADC to improve resolution. Finally, through the program, it can accurately output 10Hz sawtooth wave according to design requirements.

The sinusoidal signal generation part uses the DDS chip ICL8038 to output a sine wave, and its circuit diagram is shown in Figure 3. ICL8038 is a medium-low frequency function signal generator that can output sine, square and triangle waves simultaneously[16-18]. The sinusoidal signal generation part is designed for the commonly used frequency range, divided into 5 stops, which can generate low-loss sine waves, square waves and triangular waves of 10Hz~450KHz, and the linearity of the sine wave is adjustable, and the square wave duty cycle is adjustable, the linearity of the square wave is adjustable and the output amplitude is also adjustable. Therefore, in practical applications, it can be flexibly adjusted according to different needs.

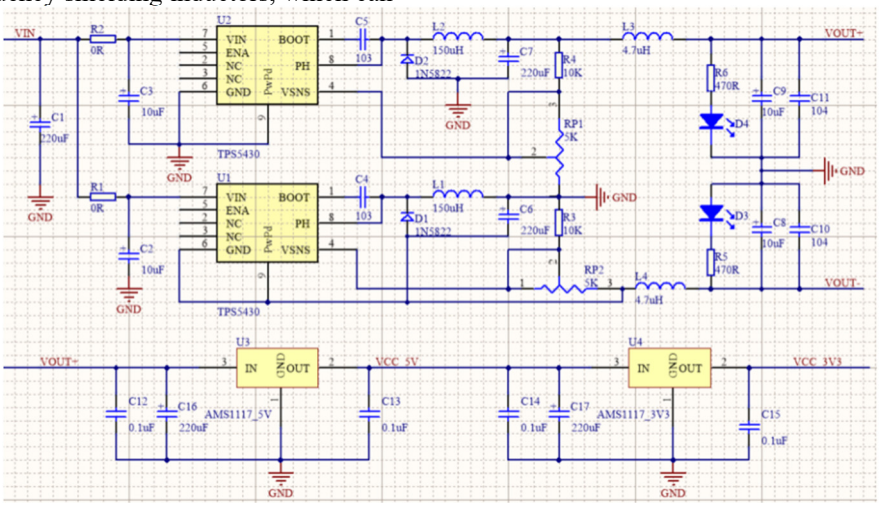


**Fig. 2.** ICL drive system power circuit.

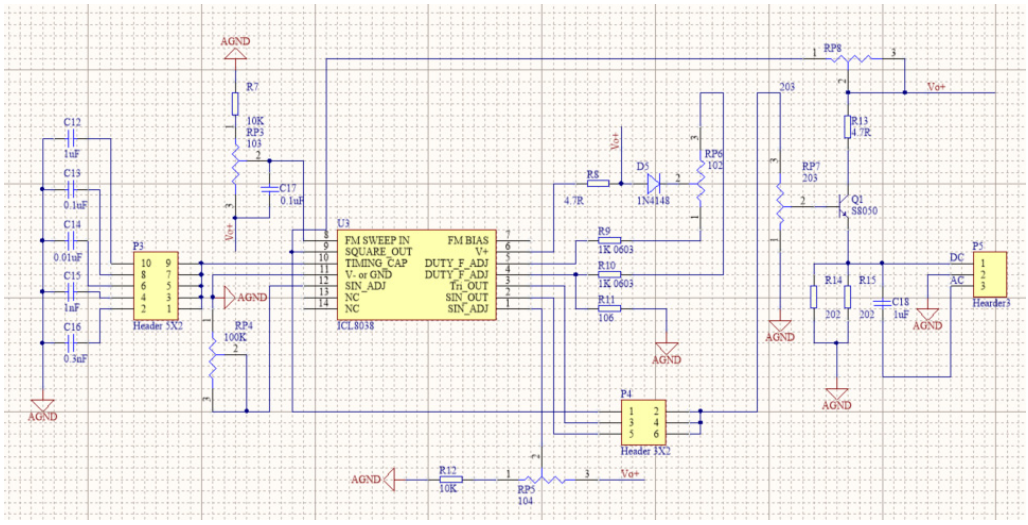


**Fig. 3.** Sine wave signal generation circuit.

### 3.3 Signal superposition and voltage-current conversion circuit

In order to generate the driving signal of the ICL, it is necessary to superimpose the sinusoidal modulation signal with the sawtooth scanning signal and convert the superimposed signal into a current driving signal. The signal superposition circuit is shown in Figure 4. The signal superposition section uses a classic analog reverse summing circuit and inverter. The reverse summing circuit is combined with the sliding rheostat to obtain a superimposed negative voltage signal with adjustable amplitude, and then the superimposed signal is converted into a positive voltage signal by an inverter. The voltage-current conversion circuit is shown in Figure 5. A positive feedback balanced voltage-current conversion circuit is used. The load can be grounded. The current output of the circuit is independent of the load, and the triode is increased in output current, thus providing a large current. This design uses a four-channel high-precision op amp OPA4277, which integrates signal superposition and voltage-current conversion circuits, reducing circuit size and improving integration[19-20].

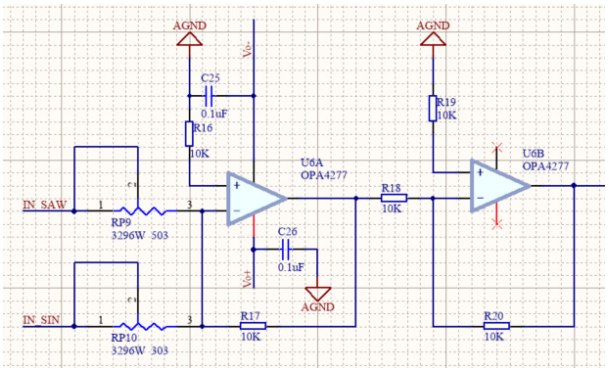


**Fig. 4.** Signal superposition circuit.

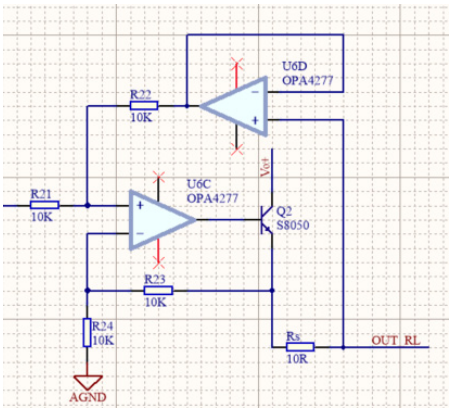


**Fig. 5.** Voltage-current conversion circuit.

### 3.4 Signal superposition and voltage-current conversion circuit simulation verification

Multisim 14 is used to simulate and verify the signal superposition and the voltage-current conversion circuit. Multisim is a SPICE simulation software from National Instruments (NI). It has the advantages of interactive simulation interface, WYSIWYG (What You See Is What You Get) development environment, virtual instrumentation and so on[21-22]. Use Multisim to interactively build the schematic of the signal superposition and voltage-current conversion circuit, and use the same parameters and models as the above circuit, and build the circuit diagram as shown in Figure 6. The virtual function signal generator is set up according to the parameters required by the laser driving signal, the signal is input to the simulation circuit, the circuit is simulated, and the simulation results of signal superposition and voltage-current conversion are checked with the virtual oscilloscope. The simulation results are shown in Figure 7. The simulation results show that the signal superposition and voltage-current conversion circuits are feasible and meet the needs of laser driving.

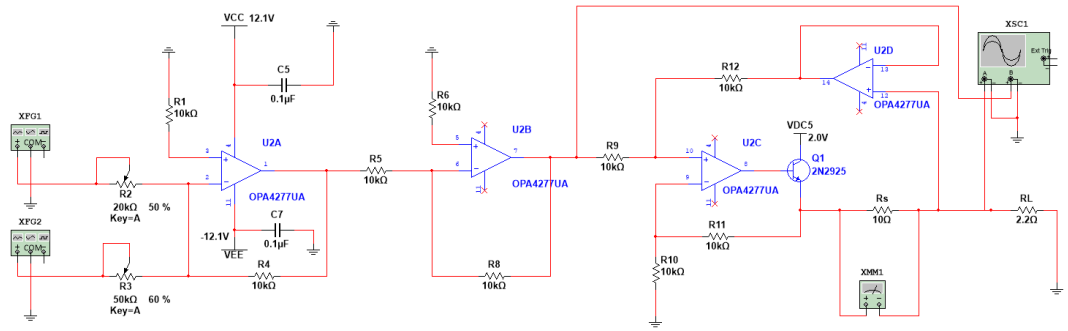


**Fig. 6.** Signal superposition and voltage-current conversion simulation circuit diagram

.

(a)

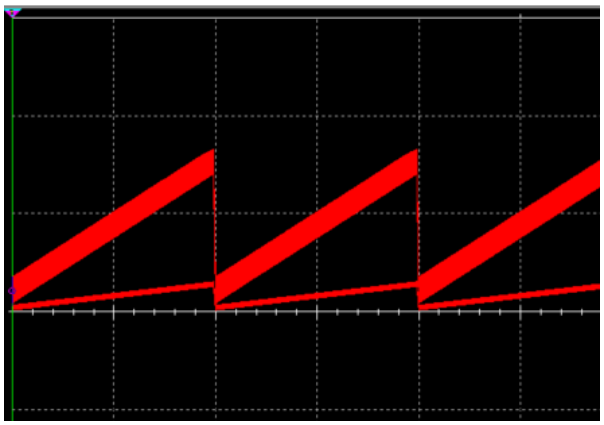

(b)

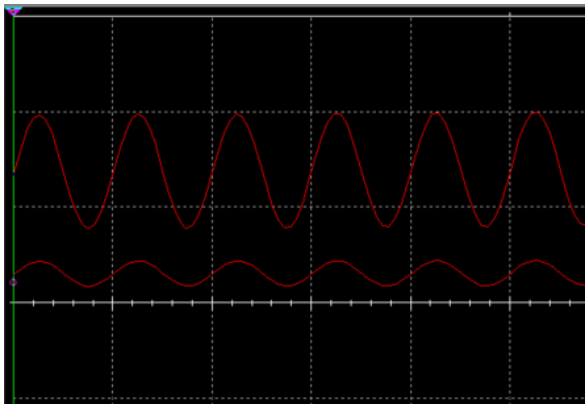

**Fig. 7.** Simulation results of signal superposition and voltage-current conversion circuits, wherein (a) the upper part of the figure is the waveform of the signal after the sawtooth scan signal and the sine wave modulation signal are superimposed. The lower part of the figure is the current drive signal converted by the voltage-current conversion circuit. Figure (b) is obtained by enlarging the figure (a).

## 4 Experimental result

The drive PCB of the $N_2O$ gas detection system is shown in Figure 8. Based on this driver board, the feasibility and stability verification test of the ICL laser drive is performed. A DFB-ICL (nanoplus Nanosystems and Technologies GmbH) emitting at ~4.47 μm was utilized as the excitation source for $N_2O$ detection. Absorptions of the mid-infrared radiations by the $N_2O$ gas, are quantifed using an HgCdTe detector (Vigo Systems, PVI-2TE-5) cooled by TEC. Detector signals are fed into a lock-in amplifier (Stanford Research Systems , SR830), which can be used to extract the second harmonic signal. At room temperature (25 °C), after the laser is stable, the driving current is set to 55 mA, and the driving current is measured every 2 minutes for 1 hour. The experimental results are shown in Figure 9. As can be seen from Figure 9, the ICL laser fluctuated slightly within a range of 55 mA in the test time of 1 hour. According to the test data, the relative error is 0.46%, which meets the system requirements.

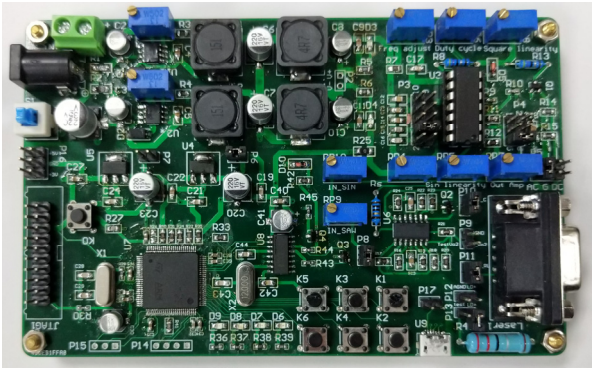

**Fig. 8.** The drive PCB of the $N_2O$ gas detection system.

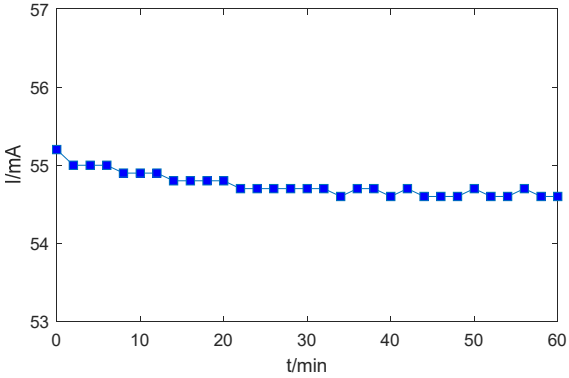


**Fig. 9.** ICL drive current stability test curve.

At room temperature (25 °C), after the laser, detector, lock-in amplifier, etc. are stable, a 10 Hz sawtooth scan signal and 10 KHz sinusoidal modulation signal are generated according to the driving requirements through the program and the sliding varistor control system.

After the signal superposition and V/I conversion, the driving signal is obtained and viewed by an oscilloscope. The result is shown in the upper part of Figure 10. After the lock-in amplifier, the second harmonic obtained is shown in the lower part of Figure 10. It can be seen from Figure 10 that the ICL driving circuit can well drive the ICL laser to meet the needs of the system.

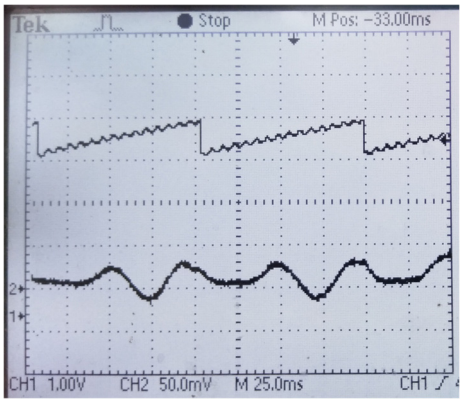


**Fig. 10.** The upper part of the figure is the measured ICL drive signal, and the lower part of the figure is the measured second harmonic.

## 5 Conclusions

This design completed the development of a driver circuit of $N_2O$ gas detection system based on tunable interband cascade laser. Experiments show that the parameters of the drive system are flexible and convenient, and the generated drive signal is stable, which can well meet the needs of the drive circuit of the $N_2O$ gas detection system based on the tunable interband cascade laser. The system has good versatility. It can be easily applied to other lasers by adjusting the scanning interval and frequency of the sawtooth signal of the driving system and adjusting the amplitude and frequency of the sine wave to meet the needs of various TDLAS gas detection systems.

## Acknowledgements

This work was supported by National key research and development program of China (2016YFD0700202).

## References

1. R.A. Rw, D. Js , Portmann, Science **326**, 123 (2009)
2. Y. Huang, Quaternary Sci. **26**, 722 (2006)
3. H. Akiyama, X.Y. Yan, K. Yagi, S.G. Haberle, H. Behling, L. Dupont, W. Kirleis, Glob. Change Biol. **16**, 1837 (2010)
4. A. Hou, G. Chen, O.V. Cleemput, Chinese J Appl. Ecol. (1998)
5. I. Vurgaftman, R. Weih, M. Kamp, J.R. Meyer, C.L. Canedy, C.S. Kim, M. Kim, W.W. Bewley, C.D. Merritt, J. Abell, J. Phys. D: Appl. Phys. **48**, 123001 (2015)
6. I. Vurgaftman, W.W. Bewley, C.L. Canedy, C.S. Kim, M. Kim, C.D. Merritt, J. Abell, J.R. Lindle, J.R. Meyer, Nat. Commun. **2**, 585 (2011)
7. C.L. Canedy, W.W. Bewley, J.R. Lindle, C.S. Kim, M. Kim, I. Vurgaftman, J.R. Meyer, Appl. Phys. Lett. **88**, 479 (2006)
8. M. Lackner, Rev. Chem. Eng. **23**, 65 (2007)
9. Y. Lu, W. Liu, J. Liu, R. Kan, Z. Xu, R. Jun, Y. Dai, Chinese J. Lasers **42**, 305 (2015)
10. R. Sur, K. Sun, J.B. Jeffries, R.K. Hanson, R.J. Pummill, T. Waind, D.R. Wagner, K.J. Whitty, Appl. Phys. B, **116**, 33 (2014)
11. J.J. Xie, Comp. Knowl. & Tech. (2017)
12. X. Miao, Elec. Meas. Tech. (2011)
13. D.Z. Sun, W.X. Wang, S. Jiang, F.B. Kong, Elec. Des. Eng. (2010)
14. F.F. Yu, L.G. Guo, L.G. Li, Ind. & Mine Auto. (2014)
15. Y. Yang, Y. Jia, C. Rong, Y. Wang, Y. Zhu, Microcomp. & Its Appl. (2015)
16. B. Bai, Microcont. & Embe. Sys. (2010)
17. S. Yang, T. Fei, D. Luan, Shaa. Elec. Power (2016)
18. C.H. Hu, Y. Chen, B.X. Sun, G.R. Zhai, Appl. Mech. & Mate. **599**, 1531 (2014)
19. Y. Yang, G. Wang, Y. Cui, D. Tao, T. Lin, F. Jia, J Agr. Mech. Rese. (2016)
20. B. Qiu, F. Jia, B. Deng, L. Wang, H. Lu, Tran. Chinese Soci. Agr. Mach. **45**, 99 (2014)
21. N. Zhang, X.F. Xin, Mode. Elec. Tech. **16**, 1178 (2010)
22. S. Feng, Y.S. Jiang, X. Yao, L.C. Wang, J Appl. Opt. **69**, 679 (2010)